Available online at www.sciencedirect.com
ScienceDirect
Journal of Catalysis 256 (2008) 84–94
JOURNAL OF CATALYSIS
www.elsevier.com/locate/jcat

Oxidative dehydrogenation of propane: Differences between N_2O and O_2 in the reoxidation of reduced vanadia sites and consequences for selectivity

Xavier Rozanska [a], Evgenii V. Kondratenko [b], Joachim Sauer [a,*]

[a] *Humboldt Universität zu Berlin, Institut für Chemie, Unter den Linden 6, D-10099 Berlin, Germany*
[b] *Leibniz-Institut für Katalyse e.V. an der Universität Rostock, Aussenstelle Berlin, Richard-Willstätter-Str. 12, D-12489 Berlin, Germany*

Received 12 October 2007; revised 27 February 2008; accepted 1 March 2008

Abstract

The role of vanadyl and peroxovanadate oxygen species in the oxidative dehydrogenation of propane (ODP) was analyzed by density functional theory (DFT). The dehydrogenation of C_3H_8 to C_3H_6 and the oxidation of C_3H_6 occurred over vanadyl oxygen of VO_x species, yielding reduced VO_x species. The vanadyl oxygen species were restored via reoxidation of reduced VO_x species with O_2 and N_2O. The ODP reaction with N_2O occurred via a $V^V(d^0)/V^{III}(d^2)$ redox couple, whereas both $V^V(d^0)/V^{IV}(d^1)$ and $V^V(d^0)/V^{III}(d^2)$ redox cycles were active with O_2. O_2 was a more active oxidizing agent than N_2O. Peroxovanadates as precursors of vanadyl species were formed on reoxidation of reduced vanadium oxide species with O_2, but not with N_2O. Peroxovanadates were highly reactive for propene oxidation. The absence of peroxovanadates may explain the superior performance of N_2O compared with O_2 in the selective ODP reaction over highly dispersed VO_x species.

Keywords: Oxidative dehydrogenation; Oxidation; Propane; Propene; Nitrous oxide; DFT; Reaction mechanism; Selectivity; Oxygen species

1. Introduction

Among the catalysts for which high propene selectivity has been achieved in the oxidative dehydrogenation of propane (ODP) are supported vanadium [1–3] and molybdenum oxide-based [4] materials. But with O_2 as an oxidizing agent, high propene selectivity (>80%) is observed only at low propane conversion (<2%). Recent studies of the ODP reaction over differently loaded VO_x/γ-Al_2O_3 [5] and VO_x/MCM-41 [6] catalysts have shown that propene selectivity is significantly improved when the reaction is performed with N_2O instead of O_2. The effect of N_2O on product selectivity has been previously observed in the oxidative coupling of methane [7–9], in the transformation of benzene to phenol [10], and in the oxidation of ethylene to ethyleneoxide [11]. Although the use of N_2O is economically unattractive because of its high cost and the product dilution by N_2, understanding the origin of the superior selective performance of N_2O compared with O_2 may help identify selective and nonselective elementary processes. This knowledge is of high scientific and industrial interest, because it may aid in the design of catalytic materials performing selectively with O_2.

One possible explanation for the high propene selectivity in the ODP reaction with N_2O over vanadium-based catalysts was given previously [5,6]: N_2O reoxidizes reduced VO_x species more slowly than O_2. This results in a higher degree of reduction of surface VO_x species and a lower density of active oxygen species, which may favor selective propane conversion to propene over consecutive propene oxidation to carbon oxides. The nature of oxygen species formed during reoxidation of reduced vanadium oxides by O_2 also may play a role [12].

The present contribution aims to further elucidate the role of various oxygen species in the elementary steps of ODP by density functional theory (DFT). We considered both lattice oxygen species in supported vanadates, such as vanadyl oxygen or bridging oxygen, and (nonlattice) oxygen species, such as superoxo and peroxo species formed on reoxidation of reduced vanadium oxide sites.

* Corresponding author.
E-mail addresses: tgakxr@chem.tue.nl (X. Rozanska), js@chemie.hu-berlin.de (J. Sauer).

0021-9517/$ – see front matter
doi:10.1016/j.jcat.2008.03.002

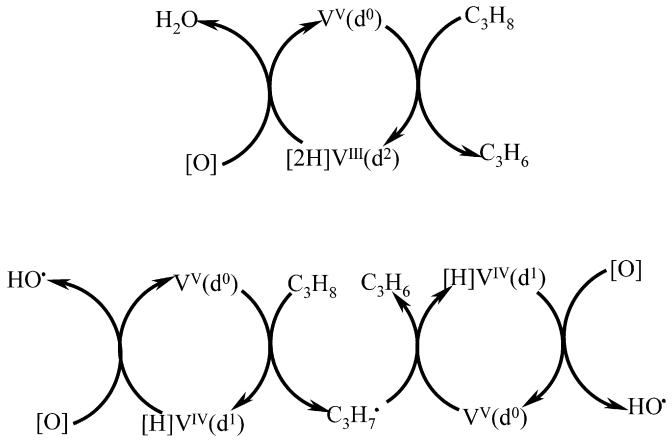

Fig. 1. Redox cycles for the oxidative dehydrogenation of propane by supported vanadium oxide.

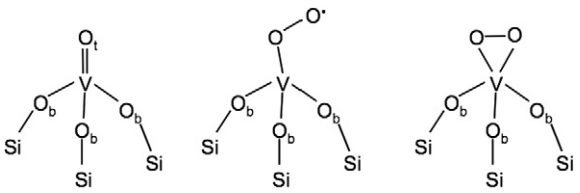

Formula 1.

We performed DFT calculations on elementary steps of the oxidation of propane and propene. The latter process contributes to the loss of propene selectivity.

A previous DFT study of the ODP mechanism [21] has demonstrated that the first and rate-limiting step is hydrogen abstraction from propane, leading to a surface propyl radical coupled to a $HOV^{IV}(O–)_3$ surface site. Propene is formed after a second hydrogen abstraction, leaving either a $V^{III}(O–)_3$ site if it occurs at the same $HOV^{IV}(O–)_3$ site or two $HOV^{IV}(O–)_3$ surface sites if it occurs at another $O{=}V^{V}(O–)_3$ surface site (Fig. 1). Consequently, we do not restrict our study to the $V^{V}(d^0)/V^{III}(d^2)$ redox couple, but also consider the $V^{V}(d^0)/V^{IV}(d^1)$ redox couple.

2. Models and methods

As in previous studies [21,22], here we adopted vanadyl-exchanged silsesquioxanes as models of monomeric ***1*** and dimeric ***49*** vanadium oxide species supported on silica. We also show that the "minimal" $O{=}V(OH)_3$ model ***5*** yielded very similar results. Because that model is computationally less demanding, we adopted it for a systematic study of different reaction mechanisms on monomeric sites. Hydrogen atoms have proven to be very effective terminating atoms for silica models [39], but not necessarily for other oxides. Therefore, the small models are not suited for studying the effect of different supports on the activity of supported vanadia sites.

Our DFT calculations used the hybrid B3LYP functional [13,14] with triple-ζ plus polarization basis sets (TZVP) [15] on all atoms, along with the Turbomole 5.7 code [16–19]. The optimized structures were characterized by frequency calculations.

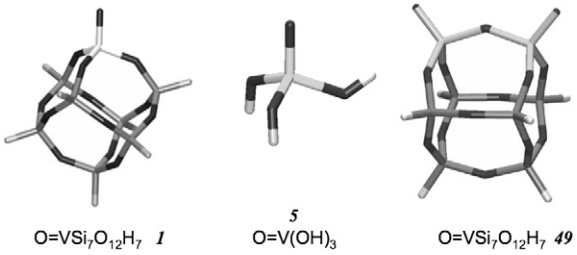

Formula 2.

All energies include zero-point vibrational energies unless otherwise stated.

Unrestricted Kohn-Sham (UB3LYP) was used for systems with triplet and open-shell singlet (broken-symmetry) spin states. Spin-projection was applied to obtain the singlet energy from the broken-symmetry and triplet energies as described previously ([20–22]; also see Eq. (5) of Ref. [21]). We report the expectation value of the total spin operator only if it deviated significantly (>0.02) from the value of the corresponding pure spin state.

Gibbs free energies were calculated within the harmonic oscillator-rigid rotor-ideal gas approximation. The rigid cluster model was adopted; that is, the translational and rotational degrees of freedom of the clusters representing the surface site were not considered when evaluating the Gibbs free energies. This allowed a more direct comparison between the values obtained with cluster models of different sizes, namely the monomeric $O{=}V(OH)_3$ and $O{=}VSi_7O_{12}H_7$ models, as well as the $(O{=}V)_2Si_6O_{12}H_6$ dimer model.

3. Results

We start with a comparison of the two different model sizes for the ODP intermediates, then consider reoxidation of $V^{III}(O–)_3$, $HOV^{IV}(O–)_3$, and $H_2O{\cdot}V^{III}(O–)_3$ species by N_2O and O_2. Finally, we analyze the reactivity and selectivity of oxygen species formed on N_2O and O_2 interaction with the reduced vanadium sites in propane and propene oxidation.

3.1. ODP Intermediates: Comparison of models

Fig. 2 shows intermediates resulting from the reaction of propane with isolated $O{=}V(O–)_3$ species for the silsesquioxane ($VSi_7O_{12}H_7$) models (***1***–***4***) and the $O{=}V(OH)_3$ models (***5***–***8***). Similar relative energies and Gibbs free energies were obtained with both types of cluster models (Table 1). Along the reaction path, the deviations varied between −9 and +12 kJ/mol. For the transition structure of the first hydrogen abstraction, the barrier for the small model (see Section 3.7.1, ***59***‡ in Table 9) deviated by <6 kJ/mol from the result for the full silsesquioxane model [21].

3.2. Reoxidation of $V^{III}(d^2)$ species

Fig. 3a shows the reaction pathways for the reoxidation of reduced $V^{III}(d^2)$ sites with N_2O and O_2 for both the $VSi_7O_{12}H_7$ (***4***) and $V(OH)_3$ models (***8***). Table 2 reports the energies for

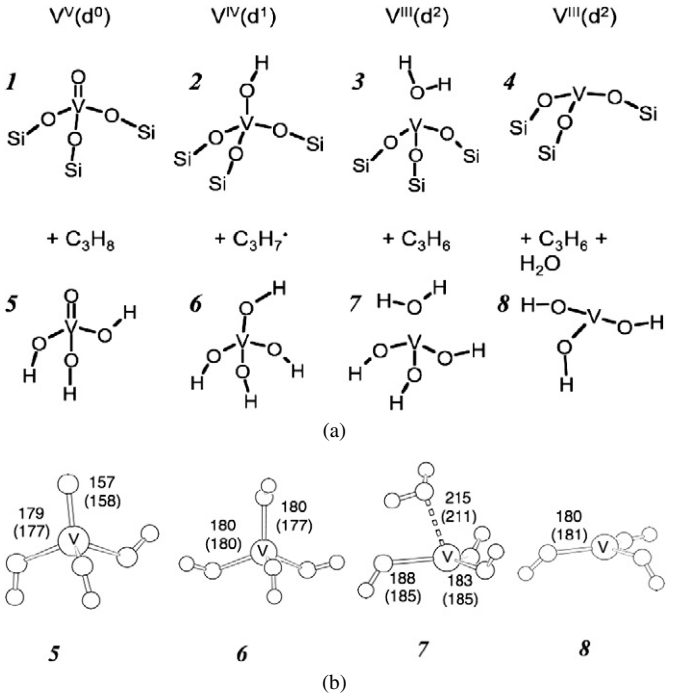

Fig. 2. (a) Intermediates in the oxidative dehydrogenation of propane by monomeric vanadium oxide sites. (b) Bond distances are in pm for models ***5–8***, values in parenthesis are for the respective silsesquioxane models ***1–4*** [21].

Table 1
Energies at 0 K, E_{ZPE}, and Gibbs free energies at T K, G_T, in kJ/mol for intermediates in the oxidative dehydrogenation of propane by O=V(O–)$_3$

Label[a]	E_{ZPE}	$G_{600\ K}$	$G_{800\ K}$
1 + C_3H_8	0	0	0
2 + $C_3H_7^\bullet$	143	125	115
^{t}***3*** + C_3H_6	94	73	62
^{t}***4*** + C_3H_6 + H_2O	180	79	42
2 × ***1*** + C_3H_8	0	0	0
2 × ***2*** + C_3H_6	53	36	27
5 + C_3H_8	0	0	0
6 + $C_3H_7^\bullet$	139	124	116
^{t}***7*** + C_3H_6	106	92	85
^{t}***8*** + C_3H_6 + H_2O	172	61	20
2 × ***5*** + C_3H_8	0	0	0
2 × ***6*** + C_3H_6	44	34	28

[a] Superscript t denotes triplet spin state.

N_2O, which can adsorb via N or O onto V. The ONN·V^{III}(d^2) complex (***9***, ***13***) was more stable than the NNO·V^{III}(d^2) complex (***10***, ***14***), but N_2 formation and restoration of the vanadyl group occurred by decomposition of the latter via a single transition structure (^{11}***11***‡, ^{15}***15***‡) with an energy barrier of around 30 kJ/mol. The reaction was exothermic, with products (***12*** and ***16***) around 360 kJ/mol more stable than the initial state.

The similar energies obtained with the two cluster models (deviations between −8 and +17 kJ/mol) confirmed that O=V(OH)$_3$ is a valid model for isolated VO_x species on SiO_2 supports. Thus, we used this model to conduct a detailed analysis of the electronic structures involved in the reoxidation process (Fig. 4). The reoxidation started on the triplet potential energy surface and arrived at the (closed shell) singlet state, ^{s}***16***. Spin-crossover [23,24] occurred after ^{t}***15***‡. We optimized the structures ***14***, ***15***‡, and ***16*** on both the triplet (superscript t) and broken-symmetry potential energy surfaces; Table 2 gives the energies. The open-shell singlet energies (superscript "s") were obtained by spin projection using the triplet energies at the broken-symmetry structure.

Compared with the reoxidation of V^{III}(d^2) by N_2O, the reoxidation with O_2 was straightforward. No energy barrier could be localized with B3LYP. Figs. 3a and 5 illustrate different intermediates obtained for different spin states. When O_2 in the triplet state interacted with the V^{III}(d^2) site, which also was in the triplet ground state, the spins could couple into an (open-shell) singlet, a triplet, or a quintet state. In the latter, $^tO_2$ was bound weakly to ^{t}V^{III}(d^2) (^{q}***17*** and ^{q}***20***, Table 3). In the open-shell singlet and triplet states, a superoxovanadate could form that was around 110 kJ/mol below the entrance channel (^{t}***18*** and ^{t}***21***). Only in the singlet state could ***18/21*** further evolve and reach a peroxovanadate species in the closed-shell singlet state (^{s}***19*** and ^{s}***22***), which was around 147 kJ/mol below the entrance channel.

In terms of the Gibbs free energy, the energy gain from peroxovanadate formation is partially or totally compensated for by the loss of rotational and translational entropy of O_2 as it binds onto the surface. According to our DFT results, the surface peroxovanadate should decompose spontaneously into O_2 and the reduced V^{III} site above 800 K at 1 bar of O_2 (Table 3). This means that peroxovanadate and O_2 + V^{III}(d^2) are in equilibrium at typical temperatures of the ODP reaction (700–773 K).

We considered two routes for the decomposition of peroxovanadate: formation of vanadyl and molecular oxygen in the gas phase, or reaction with a second V^{III}(d^2) site to yield two vanadyl sites,

$$O_2V(O–)_3 \rightarrow [O{=}V(O–)_3 + O] \rightarrow O{=}V(O–)_3 + \frac{1}{2}O_2 \qquad (1)$$

and

$$O_2V(O–)_3 + V(O–)_3 \rightarrow [O{=}V(O–)_3 + O + V(O–)_3] \rightarrow 2O{=}V(O–)_3. \qquad (2)$$

For both reactions, we considered the decomposition of peroxovanadate into vanadyl and atomic oxygen as a hypothetical transition state. This decomposition most likely occurrs with a continuous energy increase (uphill process) and requirs energies of 109 and 124 kJ/mol for ***19*** and ***22***, respectively. When the ^{t}O atom still interacted with ***5***, the decomposition energy was 115 kJ/mol (E_{ZPE} of [O·***5***] is −36 kJ/mol). No transition structure with a transition mode corresponding to the rupture of the peroxovanadate into vanadyl and an oxygen atom could be localized using a transition search method following the decomposition pathway of ***22*** into [O·***5***]. When the O atom leaves the surface, it recombines with another O atom (coming from, e.g., another peroxovanadate) to form O_2, making the process very favorable; see ***1*** + $\frac{1}{2}O_2$ and ***5*** + $\frac{1}{2}O_2$ in Table 3. This means that we may consider ***1*** + O a "transition state" for ***19*** yielding ***1*** + $\frac{1}{2}O_2$. The desorption energy ***19*** → ***1*** + O (109 kJ/mol) defines the energy barrier, and the respective desorption rate

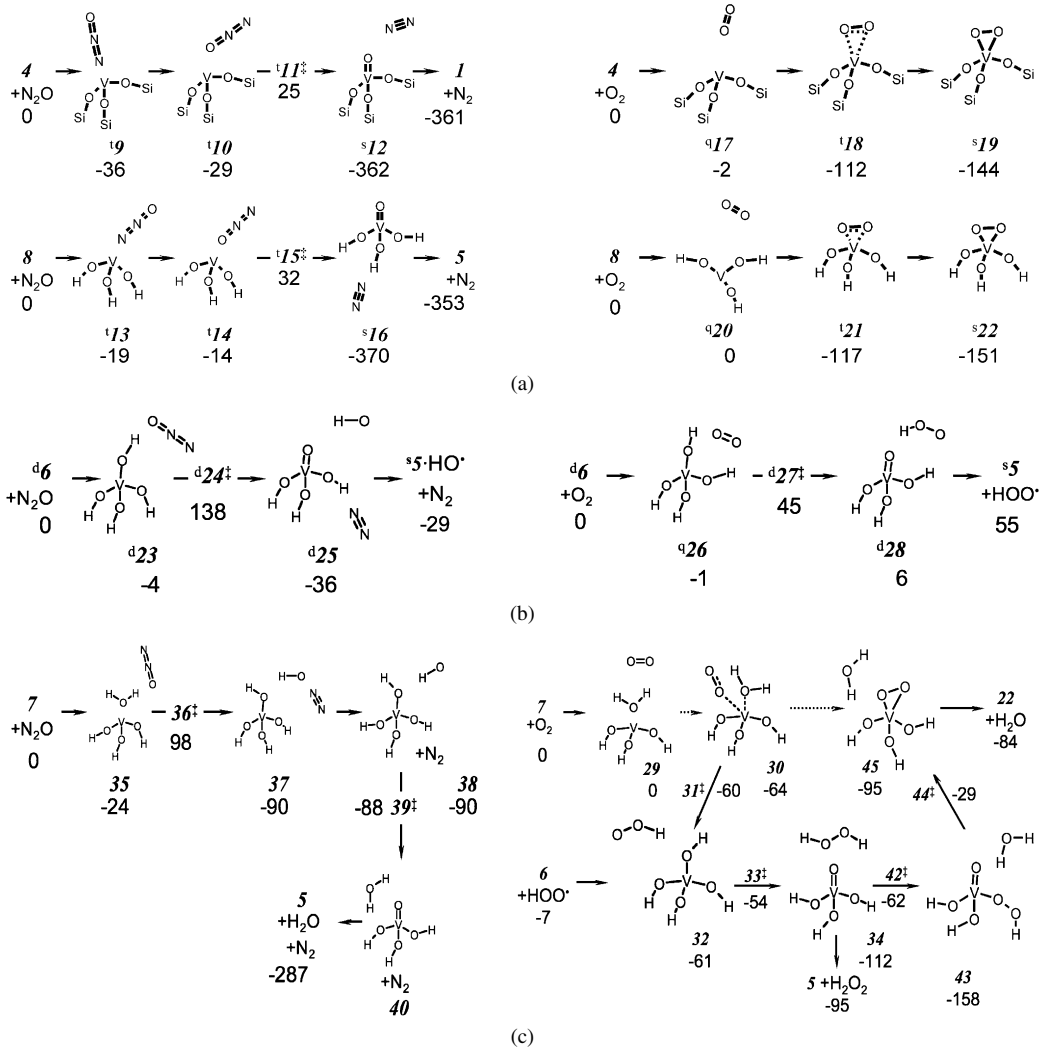

Fig. 3. Reaction pathways in the reoxidation of (a) $V^{III}(d^2)$, (b) $V^{IV}(d^1)$ and (c) $H_2O{\cdot}V^{III}(d^2)$ by N_2O and O_2. The values are energies at 0 K in kJ/mol.

(about 10^7 and 10^8 s^{-1} at 600 and 800 K, respectively; see Eq. (X) in the supplementary material of Ref. [30]) defines the decomposition rate. This does not imply that atomic oxygen existed in any measurable quantity in the system; from $\Delta G_{800\,K} = -265$ kJ/mol for the $O \rightarrow \frac{1}{2}O_2$ reaction in Table 3, it follows that the partial pressure of atomic O is 18 orders of magnitude lower than the O_2 partial pressure. It simply implies that peroxovanadate is in equilibrium with vanadate and O_2; that is, Eq. (1) is an equilibrium.

Alternatively, atomic oxygen released from the peroxo group can readsorb at a reduced $V^{III}(d^2)$ site. Also for this reaction, the desorption step would determine the rate, and Eq. (2) would define an equilibrium.

The reaction of peroxovanadate with a reduced $V^{III}(d^2)$ site also can occur by migration of oxygen atoms over the silica support via V–O–O–Si and Si–O–O–Si species instead of the desorption/readsorption of oxygen. A recent study [40] cites experimental evidence for such species and reports energy and free energy profiles for such migration. The latter were calculated by DFT, adopting a silsesquioxane model like ***1*** but with one $O{=}V(O{-})_3$ and one reduced $V^{III}(O{-})_3$ site. For peroxovanadate formation, the results were similar ($E_{el} = -180$ kJ/mol and $G_{650\,K} = -74$ kJ/mol [40]) to those reported for ***19*** in Table 3. The highest barrier for O migration with respect to the entrance channel was at $E_{el} = -51$ kJ and $G_{650\,K} = +63$ kJ/mol. This also implies rapid decomposition of about 10^3 s^{-1} at 650 K; the route via the desorption/readsorption of atomic oxygen appears to be faster, however.

In summary, in contrast to reoxidation by N_2O, reoxidation of $V^{III}(d^2)$ by O_2 exhibited no energy barrier, but the vanadyl group was not directly restored. First, peroxovanadate was formed, after which it was separated from the vanadyl group and $\frac{1}{2}O_2$ by an intrinsic barrier of about 109 kJ/mol.

3.3. Reoxidation of $V^{IV}(d^1)$ species

Reoxidation of $V^{IV}(d^1)$ sites occurred by hydrogen abstraction from ***2*** and ***6*** (Fig. 2) and simultaneous restoration of the vanadyl group (Fig. 3b). Because similar results were obtained for the $O{=}V(OH)_3$ and $O{=}V(OSi{\equiv})_3$ models, the following calculations were made only on the smaller cluster model, ***6***.

Table 2
Energies at 0 K, E_{ZPE}, and Gibbs free energies at T K, G_T, in kJ/mol for intermediates and transition structures in the reoxidation of $V^{III}(d^2)$ to $V^{V}(d^0)$ by N_2O

Label[a]	E_{ZPE}	$G_{600\,K}$	$G_{800\,K}$
^{t}***4*** + N_2O	0	0	0
^{t}***9***	−36	20	37
^{t}***10***	−25	33	50
^{t}***11***‡	25	88	108
12	−362	−367	−371
1 + N_2	−361	−374	−379
^{t}***8*** + N_2O	0	0	0
^{t}***13***	−19	55	78
^{t}***14***	−14	59	82
^{s}***14***	75(30)[b]	143(98)[b]	165(120)[b]
^{t}***15***‡	32	109	135
^{s}***15***‡	80(58)[b]	158(136)[b]	184(162)[b]
^{t}***16***	−124	−77	−64
^{s}***16***	−370	−316	−300
5 + N_2	−353	−356	−357

[a] Superscripts t and s denote triplet and singlet spin states, respectively.
[b] Singlet energies obtained by spin projection. Broken-symmetry energies in parentheses. Expectation values of the total spin are 1.0 and 0.94 for ***14*** and ***15***, respectively.

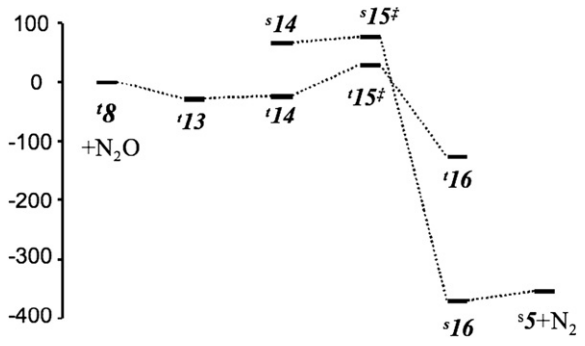

Fig. 4. Reaction energy diagram for the reoxidation of ^{t}V(O–)$_3$ by N_2O. Electronic energies in kJ/mol, see also Table 3.

When N_2O was abstracting the hydrogen, the products were N_2, OH$^•$, and O=$V^{V}(d^0)$ (***25***). The energy for adsorption of N_2O to HOV(O–)$_3$ (***23***) was slightly negative (Table 4). After crossing the transition structure ***24***‡ (energy barrier, 138 kJ/mol), the energy became negative (***25***). The entire reaction occurred on the doublet potential energy surface.

When reoxidation was achieved by O_2, the reaction products were O=$V^{V}(d^0)$ and HOO$^•$ (***28***). HOO$^•$ could reoxidize another HOV^{IV}(O–)$_3$ site to yield O=V^{V}(O–)$_3$ and H_2O_2 (***34***) via transition structure ***33***‡ with a barrier of $55 - 7 - (30 \pm 24) = 18 \pm 24$ kJ/mol (see Fig. 3c and energies in Table 5; also see Section 3.4 for the uncertainty of the energy of ***33***‡). The formed complex ***34*** could be converted via low barrier steps ***42***‡ and ***44***‡ into peroxovanadate and H_2O. This required migration of $^•$OOH on the surface to another HOV^{IV}(O–)$_3$ site or desorption/readsorption steps as discussed earlier for oxygen.

H_2O_2 itself was consumed by different processes, including reoxidation of HOV^{IV}(O–)$_3$, according to

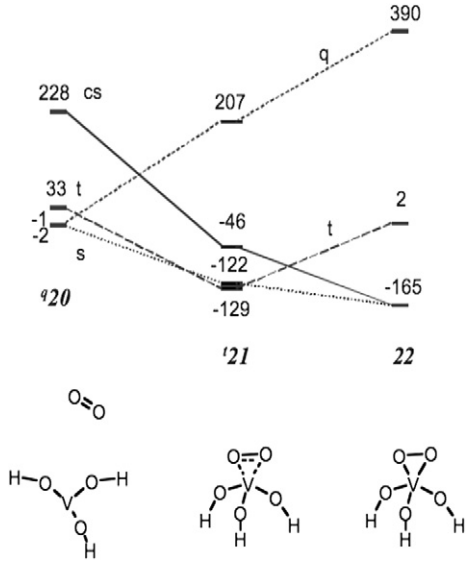

Fig. 5. Reaction energy diagram for the reoxidation of V(O–)$_3$ by O_2. The single point energies in the open (s) and closed-shell (cs) singlet, triplet (t), and quintet (q) electronic configuration of the fully optimized intermediates ***20***, ***21***, and ***22*** are indicated. The superscripts on ***20***, ***21***, and ***22*** indicate the spin assumed during the optimization of the intermediates. All values are electronic energies in kJ/mol relative to ^{t}O$_2$ + ^{t}V(O–)$_3$.

Table 3
Energies at 0 K, E_{ZPE}, and Gibbs free energies at T K, G_T, in kJ/mol of the intermediates in the reoxidation of $V^{III}(d^2)$ to $V^{V}(d^0)$ by O_2

Label[a]	E_{ZPE}	$G_{600\,K}$	$G_{800\,K}$
^{t}***4*** + O_2	0	0	0
^{s}***17***	−2	12	14
^{t}***18***	−112	−19	11
^{s}***19***	−144	−38	−2
1 + O	−35	−3	7
1 + $\frac{1}{2}O_2$	−275	−210	−258
^{t}***8*** + O_2	0	0	0
^{q}***20***	0	43	54
^{t}***21***	−117	−9	28
22	−151	−39	1
5 + O	−27	14	30
5 + $\frac{1}{2}O_2$	−267	−193	−235

[a] Superscripts s, t, q denote singlet, triplet and quintet spin states, respectively.

$$2HOV(OH)_3 + H_2O_2 \rightarrow 2O{=}V(OH)_3 + 2H_2O.$$

The E_{ZPE}, $G_{600\,K}$, $G_{800\,K}$ values were −265, −325 and −354 kJ/mol, respectively, indicating an "easy" process.

The interaction between O_2 and HOV(O–)$_3$ in the O_2·HOV(O–)$_3$ complex (***26***) was weak (Table 4) in both the high-spin (quartet) and low-spin (doublet) states. A transition structure corresponding to hydrogen transfer could be localized only on the doublet potential energy surface (***27***‡). The energy barrier was 93 kJ/mol lower than the barrier for N_2O, and the free energy barrier at 600 K was 58 kJ/mol lower, demonstrating that reoxidation of $V^{IV}(d^1)$ was much easier by O_2 than by N_2O.

Table 4
Energies at 0 K, E_{ZPE}, and Gibbs free energies at T K, G_T, in kJ/mol for intermediates and transition structures in the reoxidation of reduced $V^{IV}(d^1)$ active sites by N_2O and O_2

Label[a]	E_{ZPE}	$G_{600\ K}$	$G_{800\ K}$
^{d}***6*** + N_2O	0	0	0
^{d}***23***	−4	42	55
^{d}***24***‡	138	207	230
^{d}***25***	−36	−17	−15
^{d}***5***·HO$^•$ + N_2	−29	−49	−60
^{d}***6*** + O_2	0	0	0
^{4}***26***, ^{d}***26***	−1[b]	52	67
^{d}***27***‡	45	149	186
^{d}***28***	6	94	123
5 + HOO$^•$	55	52	52

[a] Superscripts *d* and 4 denote doublet and quartet spin states, respectively.
[b] ***26*** has virtually the same electronic energy in the quartet (4) and doublet (*d*) spin states.

Table 5
Energies at 0 K, E_{ZPE}, and Gibbs free energies at T K, G_T, in kJ/mol for intermediates and transition structures in the reoxidation of $H_2O{\cdot}V^{III}(d^2)$ by O_2

Label[a]	E_{ZPE}	$G_{600\ K}$	$G_{800\ K}$
8 + O_2 + H_2O	66	−31	−65
7 + O_2	0	0	0
^{q}***29***	0	48	61
^{s}***29***	−1[b]	51	66
^{t}***30***	−64	40	76
^{s}***30***	−69(−65)[c]	33(37)[c]	69(72)[c]
22 + H_2O	−85	−70	−64
^{t}***31***‡	−60	48	87
^{s}***31***‡	−63[b]	35	70
^{t}***32***	−61	43	79
^{s}***32***	−61[b]	42	78
^{s}***33***‡	−54(−6)[c]	33(81)[c]	63(111)[c]
^{s}***34***	−112	−32	−5
42‡	−62	50	91
43	−158	−52	−15
44a‡	31	114	142
44‡	−29	64	96
45	−95	−92	−89
22 + H_2O	−85	−70	−64
5 + H_2O_2	−95	−92	−89
6 + HOO$^•$	−7	−7	−6

[a] Superscripts *s*, *t*, *q* denote singlet, triplet and quintet spin states, respectively.
[b] Broken-symmetry energies and low spin (singlet) energies are the same within 1 kJ/mol.
[c] Energies obtained by spin projection. Broken-symmetry energies in parentheses. Expectation values of the total spin are 1.0 and 0.63 for ***30*** and ***33***‡, respectively.

3.4. Reoxidation of $H_2O{\cdot}V^{III}(d^2)$ species

Reoxidation of $V^{III}(d^2)$ with O_2 and N_2O also could proceed directly from $H_2O{\cdot}V^{III}(O–)_3$ species (see Fig. 3c). The interaction between O_2 and $H_2O{\cdot}V(O–)_3$ (***29***) was as weak as the interaction between O_2 and $V(O–)_3$ (***20***). The complex ***29*** had high-spin (quintet) and low-spin (singlet) states with similar energies, resulting from two interacting triplets. This complex evolved toward a superoxovanadate complex ***30***, with the same structure and energies in both the triplet and singlet spin states. This complex could rearrange in a more stable (by 31 kJ/mol) complex of peroxovanadate with water, ***45***. Desorption of water from ***45*** to reach peroxovanadate ***22*** (+H_2O) required only 11 kJ/mol. An additional route from ***30*** was hydrogen transfer from water to oxygen, yielding the $^•$OOH·$HOV^{IV}(d^1)(O–)_3$, complex, ***32***, a biradical that had virtually the same energy in the triplet and singlet spin states. The transition structure ***31***‡ also had the same energy on the triplet and (open-shell) singlet potential energy surfaces. At about 4 kJ/mol, the energy barrier with respect to ***30*** was very small, and the energy of ***32*** was only marginally higher than that of ***30***.

The next step along this route was hydrogen transfer from $HOV(O–)_3$ to $^•$OOH leading to the much more stable complex of H_2O_2 with $O{=}V(O–)_3$, ***34***. It existed as a singlet, and the transition structure ***33***‡ could be localized only within the broken-symmetry formalism. At 0.63, $\langle S^2\rangle$ was much smaller than 1 (Table 5), indicating strong interaction between the spins and making spin projection doubtful [21,26,27]. Taking the broken-symmetry and spin-projected energies as limits, the low-spin energy of ***33***‡ could be estimated as -30 ± 24 kJ/mol. Although the uncertainty is relatively large, the higher value is still well below the entrance channel of the reaction, indicating very fast formation of $H_2O_2{\cdot}O{=}V(O–)_3$. From this complex, H_2O_2 could be released (H_2O_2 + ***5*** was more stable than H_2O + ***22***; Table 5), and H_2O_2 formation indeed was observed in homogeneous reoxidation of vanadium oxide by O_2 [28].

A more stable intermediate $H_2O{\cdot}O{=}V(O–)_2(OO–)$ (***43***) was reached via transition structure ***42***‡ if in ***34*** a hydrogen atom was transferred from H_2O_2 to a terminal O–H group in $O{=}V(O–)_3$ at the same time that one O–V bond was broken and another one was formed; that is, –OOH became connected to V, whereas –OH was detached as H_2O. Rearrangement of $O{=}V(O–)_2(OO–)$ via H transfer and OOV ring closure through ***44***‡ yielded the H_2O·peroxovanadate complex ***45***, which was less stable than the H_2O_2·vanadate complex ***41***. From ***43***, transformation of $O{=}V(O^1–)(O^2–)(O^3O^4–)$ into $O{=}V(O^1O^3–)(O^2–)(O^4–)$ by oxygen transfer also was possible, but the energy of the respective transition structure ***44a***‡ was much higher than that of ***44***‡.

The succession of transition structures and intermediates was slightly different when the large model ***1*** was used instead of ***5*** ($O{=}V(OH)_3$). The reaction of H_2O_2 with $O{=}V(–OSi)_3$ in ***1*** yielded $O{=}V(–OSi)_2(–OOH)(HOSi)$, which recombined to $O{=}V(–OSi)_2(–OOSi)$ + H_2O and further rearranged to $(OO)V(–OSi)_3$ + H_2O. With the $O{=}VSi_7O_{12}H_7$ cluster model ***1***, the energy of $O{=}V(–OSi)_2(–OOSi)$ was 4 kJ/mol lower than that of $(OO)V(–OSi)_3$. The energy barriers on this pathway were relatively small, and the reaction could proceed in both directions depending on concentration; that is, peroxovanadate also could dissociate into vanadyl and H_2O_2 when in contact with H_2O.

Fig. 3c (left) and Table 6 show the results for the hydrogen transfers between $H_2O{\cdot}V(O–)_3$ and N_2O. N_2O was bound more strongly on $H_2O{\cdot}V(O–)_3$ compared with O_2 (***35***). The first hydrogen transfer led to a biradical (***37***). The transition structure

Table 6
Energies at 0 K, E_{ZPE}, and Gibbs free energies at T K, G_T, in kJ/mol for intermediates and transition structures in the reoxidation of $H_2O{\cdot}V^{III}(d^2)$ by N_2O

Label[a]	E_{ZPE}	$G_{600\ K}$	$G_{800\ K}$
^{t}***8*** + N_2O + H_2O	66	−31	−65
^{t}***7*** + N_2O	0	0	0
^{t}***35***	−24	33	50
^{t}***36***‡	98	171	195
^{t}***37***	−90	−66	−62
^{t}***38*** + N_2	−90	−112	−120
^{s,t}***38*** + N_2	−90[b]	−112	−120
^{s}***39***‡ + N_2	−91(−88)[c]	−109(−106)[c]	−121(−119)[c]
40 + N_2	−313	−348	−361
5 + N_2 + H_2O	−287	−388	−421

[a] Superscripts s and t denote singlet and triplet spin states, respectively.
[b] Triplet, broken-symmetry and low spin (singlet) energies are the same within 1 kJ/mol.
[c] Energies obtained by spin projection. Broken-symmetry energies in parentheses. Expectation value of the total spin is 0.95.

(***36***‡), which had a relatively high energy, existed only on the triplet potential energy surface. N_2 was bound to the vanadium oxide only via van der Waals interactions and could desorb (***38***). Van der Waals interactions are poorly described by DFT, explaining why the energies of ***37*** and ***38*** are the same. However, the free energy gain obtained by releasing N_2 from the surface was so large that N_2 desorbed immediately at reaction temperature even for realistic binding energies. The transition structure for the subsequent second hydrogen transfer from $HOV(O–)_3$ to $OH^•$ (***39***‡) to yield H_2O and $O{=}V(O–)_3$ (***40***) existed only on the broken-symmetry surface, as for the O_2 reaction pathway. Both energy and Gibbs free energy barriers are only a few kJ/mol, indicating that this second hydrogen transfer was instantaneous. The formation of ***40*** was strongly exothermic, and the Gibbs free energies of ***40*** and ***5*** shown in Table 6 indicate that water rapidly desorbed from the vanadyl.

Consequently, hydrogen transfers from $H_2O{\cdot}V(O–)_3$ to O_2 and N_2O restoring the vanadyl group were possible and occurred depending on the reaction conditions (particularly water content). The highest intrinsic energy barrier was calculated for the reoxidation with N_2O. This barrier was higher than that for the reoxidation of $V(O–)_3$ by N_2O; that is, reoxidation of $V^{III}(d^2)$ by N_2O dominated the reoxidation of $H_2O{\cdot}V^{III}(d^2)$ by N_2O.

3.5. Peroxovanadate formation

The main difference in the reoxidation of $V^{III}(d^2)$ by N_2O and O_2 is that the latter reaction yields peroxovanadate or, for hydrated sites, H_2O_2. Consequently, it is particularly important to investigate whether peroxovanadate could be generated through a reaction of vanadyl with N_2O. To the best of our knowledge, no previous theoretical or experimental data are available; we present results for this reaction in Fig. 6 and Table 7. The formation of peroxovanadate using N_2O can be safely disregarded because of the high barrier (225 kJ/mol) connected with transition structure ***47***‡.

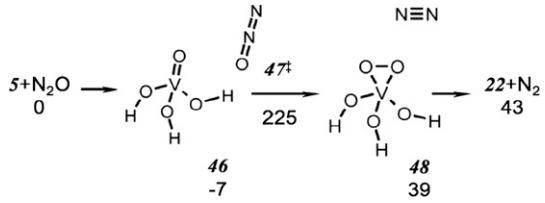

Fig. 6. Reaction pathway for the oxidation of vanadyl to peroxovanadate by N_2O. The values are energies at 0 K in kJ/mol.

Table 7
Energies at 0 K, E_{ZPE}, and Gibbs free energies at T K, G_T, in kJ/mol of intermediates and transition structures in the oxidation of vanadyl to peroxovanadate by N_2O

Label	E_{ZPE}	$G_{600\ K}$	$G_{800\ K}$
5 + N_2O	0	0	0
46	−7	36	49
47‡	225	287	306
48	39	78	88
22 + N_2	43	22	13

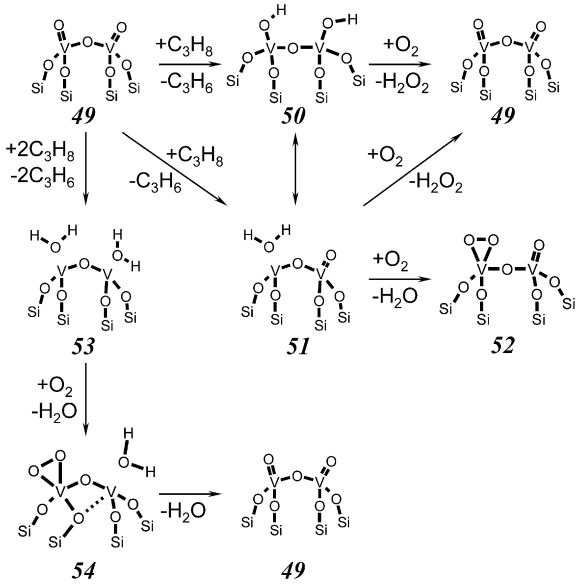

Fig. 7. ODP intermediates for dimeric vanadium oxide sites.

3.6. Reaction intermediates in ODP with a dimeric VO_x species

We do not know whether vanadium oxide supported on silica has exclusively monomeric VO_x species or if (and under which conditions) VO_x species of higher polymerization degree also are present [29]. Consequently, we explored the reoxidation of reduced dimeric vanadium oxide sites (Fig. 7) based on energies of intermediates given in Table 8. No transition structures were localized. We assumed that barriers could be similar for monomeric and dimeric sites.

We used a dimeric vanadium-exchanged silsesquioxane (***49***) [29] with a structure derived from ***1*** (Fig. 2). We considered two reaction pathways in the ODP reaction [30] (Fig. 7). According to the first of these pathways, $V^V(d^0)/V^V(d^0)$ was reduced to $V^{IV}(d^1)/V^{IV}(d^1)$ (***50***). As discussed in Section 3.3, O_2 could

Table 8
Energies at 0 K, E_{ZPE}, and Gibbs free energies at T K, G_T, in kJ/mol of intermediates in the ODP by dimeric vanadyl active sites

Label	E_{ZPE}	$G_{600\ K}$	$G_{800\ K}$
49 $+ C_3H_8 + O_2$	0	0	0
50 $+ C_3H_6 + O_2$	41	24	14
49 $+ C_3H_6 + H_2O_2$	12	0	−4
51 $+ C_3H_6 + O_2$	79	62	53
52 $+ C_3H_6 + H_2O$	32	38	38
49 $+ 2C_3H_8 + O_2$	0	0	0
53 $+ 2C_3H_6 + O_2$	194	162	146
54 $+ 2C_3H_6 + H_2O$	68	73	70
49 $+ 2C_3H_6 + 2H_2O$	−203	−295	−329

easily reoxidize $HOV^{IV}(d^1)$ (***27***‡, 45 kJ/mol). The HOO• radical formed after ***27***‡ (Fig. 3b) will immediately react with the neighboring $HOV^{IV}(d^1)$ site with a very low barrier (similarly as ***33***‡, Fig. 3c).

The reoxidation of ***50*** by N_2O was more difficult (Fig. 3b, ***24***‡, 138 kJ/mol), and the isomerization of ***50*** to ***51*** could compete with it (energy barrier, 146 kJ/mol) [29]. The reoxidation of ***51*** by N_2O and O_2 could occur before or after H_2O desorption. We described the reaction mechanisms in previous sections. Similar to monomeric vanadium oxide clusters, with O_2, the peroxovanadate ***52*** could be reached once H_2O (formed during the ODP) desorbed from $V^{III}(d^2)$. This remained unchanged regardless of whether vanadium oxide existed as monomeric species or as dimeric species. The decomposition of ***52*** into ***49*** and atomic oxygen gave a reaction energy of 113 kJ/mol (cf. 109 kJ/mol for ***19*** into ***1*** + O).

Finally, we mention the unlikely situation in which both vanadium sites in the dimer were reduced to $V^{III}(d^2)$ (***53***). The intermediate ***53*** had a much higher energy than the others, and the catalytic cycle could not reach this situation. Reoxidation of ***53*** was similar to that of the monomer. When O_2 was the reoxidizing agent, it replaced H_2O, and peroxovanadate was formed. Reoxidation of the neighboring $V^{III}(d^2)$ by the peroxovanadate site could follow different reaction pathways (after or before water desorption); all of these processes were quick and easy, considering the high activity of peroxovanadate. We conclude that the presence of dimeric vanadium oxide species on silica did not significantly alter the reoxidation reaction pathways as obtained for the monomeric species. In particular, it did not affect the differences observed between N_2O and O_2 as reoxidizing agents.

3.7. Hydrocarbon activation by peroxovanadate and vanadyl

The main difference between reoxidation of reduced VO_x species by O_2 and N_2O is that the former can form surface peroxovanadate. As shown in Section 3.2, N_2O by itself was not a strong enough oxidant to form peroxovanadate from vanadyl. Does the presence of peroxovanadate explain the poorer selectivity of O_2 in the oxidative dehydrogenation of propane? To gain some insight into this question, we considered the reaction pathways of propane (Section 3.7.1) and propene (Section 3.7.2) oxidation by surface vanadyl and peroxovanadate oxygen species.

Experimental evidence exists [6] demonstrating that the loss of selectivity in the ODP reaction over highly dispersed VO_x species on MCM-41 stems mainly from consecutive oxidation of primarily formed propene. Thus, the analysis of propene oxidation is of great importance to the design of selective catalytic materials. On the other hand, propane is the most abundant species in the system, with a concentration far higher than that of propene; therefore, the oxidation of propane by vanadyl and peroxovanadate also was examined.

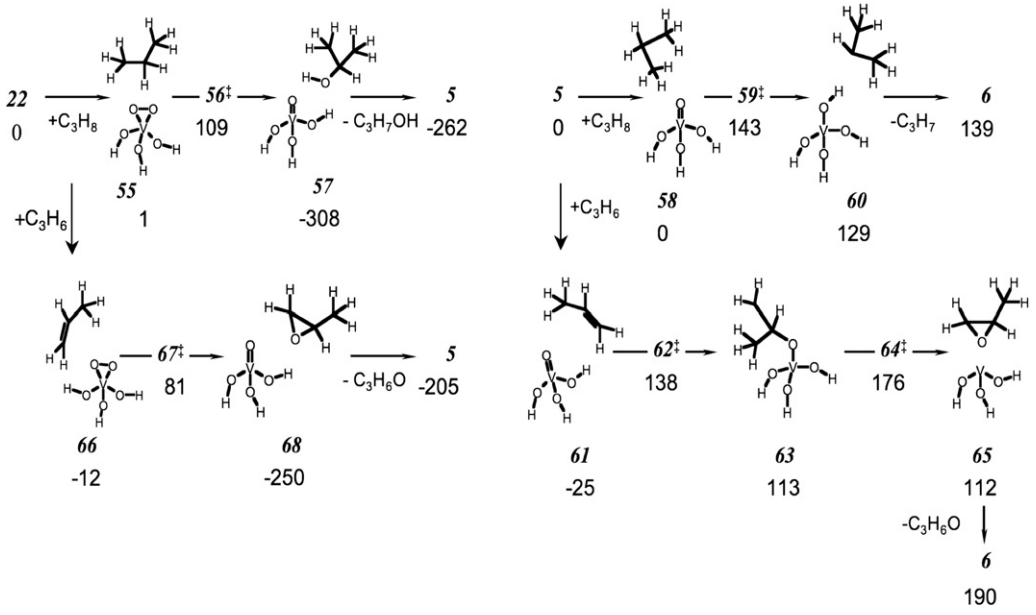

Fig. 8. Reaction pathways for the reaction of propane (top) and propene (bottom) by vanadyl (right) and peroxovanadate sites (left). The values are energies at 0 K in kJ/mol.

Table 9
Energies at 0 K, E_{ZPE}, and Gibbs free energies at T K, G_T, in kJ/mol of intermediates and transition structures for the reaction of propane with vanadyl and peroxovanadate sites

Label[a]	E_{ZPE}	$G_{600\ K}$	$G_{800\ K}$
19 $+ C_3H_8$	0	0	0
55	1	53	67
56‡	109	207	238
57	−308	−221	−194
5 $+ C_3H_7OH$	−262	−264	−265
5 $+ C_3H_8$	0	0	0
58	18	74	89
^{s}***59***‡[b]	123(143)[b]	208(228)[b]	233(253)[b]
^{s}***60***	127[c]	191	207
^{t}***60***	129	198	216
6 $+ C_3H_7^{\bullet}$	139	124	116
TS‡[d]	199	286	310
7 $+ C_3H_6$	107	93	85

[a] Superscripts s and t denote singlet and triplet spin states, respectively.
[b] Energies obtained by spin projection. Broken-symmetry energies in parentheses. Expectation value of the total spin is 0.75.
[c] Broken-symmetry energy and low spin (singlet) energy are the same within 1 kJ/mol.
[d] ***TS***‡ is the transition structure leading to $[C_3H_6{\cdot}H_2O{\cdot}V(O{-})_3]$ from ^{t}***52*** [21].

3.7.1. Activation of propane

It has been shown that surface vanadyl sites can abstract hydrogen from propane in a single step [21]. The reaction mechanisms and energies given in Fig. 8 and Table 9, respectively, show that also is true for peroxovanadate sites. After propane adsorption (***55***), the peroxo-group abstracted hydrogen from propane, and a vanadyl group was formed. Examination of the transition mode in ***56***‡ indicates formation of a propyl and a hydroxyl group, but this intermediate could not be localized as a stationary point, and its structure immediately evolved toward isopropanol and a vanadyl site (***57***). The energy barrier for isopropanol formation was 108 kJ/mol with respect to ***55***, demonstrating that the peroxovanadate group was much more active than the vanadyl group, for which a barrier of 143 kJ/mol was obtained (***59***‡). This finding suggests that peroxovanadate species will not persist under ODP conditions. The contribution of different channels to the peroxovanadate decomposition, such as releasing O_2 or reacting with propane, will depend on the specific reaction conditions. The formation of isopropanol and vanadyl (***57***) was strongly exothermic and yielded sufficient energy to overcome the intrinsic barrier of about 140 kJ/mol for further oxidation of isopropanol to acetone [22], opening the path to CO_x. Isopropanol also can dehydrate if $V^{III}(d^2)$ sites are available [21].

Because the results for the silsesquioxane model have been published previously [21], for comparison, Table 9 and Fig. 8 present only the most relevant results for the ODP by vanadyl sites for the small $O{=}V(OH)_3$ model. The first hydrogen abstraction (***59***‡) is the rate-determining step, with an energy barrier of 133 ± 10 kJ/mol. It leads to formation of a propyl radical attached to $HOV^{IV}(d^1)$ (***60***) as a high-energy intermediate that gives propene and $H_2O{\cdot}V^{III}(d^2)$ via several competitive reaction routes. We mention one of the dominant transition structures, ***TS***‡ in Table 9 [21,30].

We note that surface $HOO^{\bullet}$, the primary product of the reoxidation of $HOV^{IV}(d^1)$ sites by O_2, also can abstract hydrogen from propane, yielding H_2O_2 and propyl radical (estimated energy barrier, 65 kJ/mol). Thus, both surface vanadyl and peroxovanadate species are able to activate propane, but peroxovanadate is more reactive, and the products are different (propene and isopropanol, respectively). Isopropanol can be further oxidized to acetone by the vanadyl group, or it can become dehydrated by $V^{III}(d^2)$.

Table 10
Energies (kJ/mol) of the intermediates and transition structures for the reaction of propene with vanadyl and peroxovanadate sites

Label[a]	E_{ZPE}	$G_{600\ K}$	$G_{800\ K}$
22 $+ C_3H_6$	0	0	0
66	−12	67	90
67‡	81	186	219
68	−250	−157	−127
5 $+ C_3H_6O$	−205	−204	−202
19 $+ C_3H_6$	0	0	0
5 $+ C_3H_6$	0	0	0
61	−25	52	76
^{s}***62***‡	117(138)[b]	215(236)[b]	246(267)[b]
^{t}***63***	113	206	234
^{t}***64***‡	176	277	310
^{t}***65***	112	207	237
^{t}***6*** $+ C_3H_6O$	190	174	168

[a] Superscripts s and t denote singlet and triplet spin states, respectively.
[b] Energies obtained by spin projection. Broken-symmetry energies in parentheses. Expectation value of the total spin is 0.75.

3.7.2. Activation of propene

The lower part of Fig. 8 shows the mechanisms of the reactions of peroxovanadate and vanadyl sites with propene. Both yielded propene oxide, but the energy barriers again were much lower for the peroxovanadate species. The energies of the intermediates and transition structures are reported in Table 10.

The oxidation of propene by a vanadyl group was not an easy process. After adsorption to the vanadyl group (***61***), propene chemisorbed through the broken-symmetry transition structure ***62***‡. The energy barrier of 127 ± 11 kJ/mol was similar to the barrier for hydrogen abstraction from propane (***59***‡; 133 ± 10 kJ/mol). The biradical intermediate ***63*** converted into the epoxide with an energy barrier of 176 kJ/mol (***64***‡). Formation of acetone from ***63*** required overcoming an even higher barrier. The conversion of propene to propene oxide (***65***) was endothermic. In contrast, the conversion of propene by peroxovanadate was strongly exothermic (***68***; −250 kJ/mol). After propene adsorption onto the peroxovanadate species (***66***), oxygen transfer (***67***‡) led immediately to propene oxide and a vanadyl species (***68***) with a barrier of only 93 kJ/mol.

To summarize, peroxovanadate and vanadyl can oxidize propene to propene oxide; however, peroxovanadate does it with a significantly lower energy barrier. Whatever species it comes in contact with (be it propene, propane, or water), that species is oxidized, and vanadyl is restored. Formation of

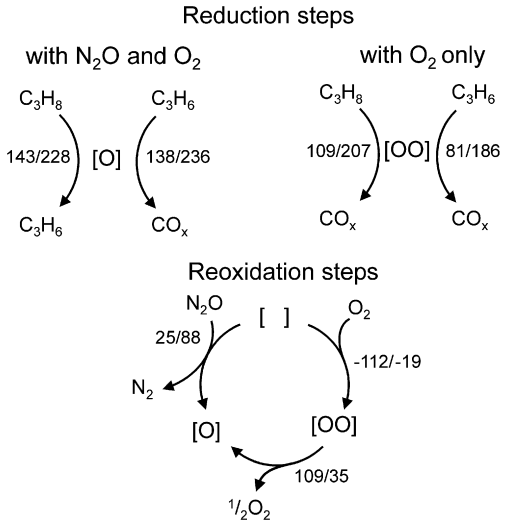

Fig. 9. ODP reaction pathways on vanadyl (left) and peroxovanadate species (right). Reoxidation of reduced VO_x sites by N_2O or O_2 is shown at the bottom. [ ], [O], and [OO] denote the reduced VO_x site, the vanadyl oxygen, and the peroxo species, respectively. The numbers are the calculated zero-point energy/free energy (600 K) barriers for the initial steps leading to the corresponding products.

propene oxide is strongly exothermic, opening the route to the full oxidation of hydrocarbons.

4. Discussion

Fig. 9 shows a simplified scheme of ODP product formation in the presence of O_2 and N_2O as emerging from the present DFT calculations (Fig. 9). The numbers given are the calculated energy/Gibbs free energy barriers (600 K) for the initial steps leading to the respective products. Independent of the oxidizing agent (O_2 or N_2O), C_3H_6 is formed by successive abstraction of two H atoms from C_3H_8 by VO_x species, which are reduced in the process. This agrees with previous experiments on the ODP reaction over various vanadium-based catalytic materials [5,31–37]. DFT calculations suggest the involvement of the vanadyl oxygen atom of VO_x species in the rate-determining step of propane activation [21,30] and also, as we have shown, in the further oxidation of propene, ultimately yielding CO_x species.

Reoxidation of the reduced VO_x species is shown in the lower part of Fig. 9. According to the DFT calculations discussed in Sections 3.2–3.4, O_2 can easily oxidize vanadium +III and +IV species, whereas N_2O reoxidizes vanadium +III species. The significantly higher barriers demonstrate that N_2O is a less-reactive oxidizing agent than O_2. This theoretical result agrees with an earlier experimental kinetic analysis of reoxidation of reduced VO_x species over VO_x (2.7 wt%)/MCM-41 by O_2 and N_2O [38] and demonstrates that the rates of propane consumption and propene formation over VO_x/MCM-41 [6] and VO_x/γ-Al_2O_3 [5] are lower with N_2O than with O_2.

N_2O and O_2 also differ in terms of the nature of oxygen species formed on reoxidation of reduced VO_x species. N_2O selectively restores vanadyl oxygen in the reduced VO_x species, whereas O_2 can form peroxovanadates, which then decompose into vanadyl and oxygen. The latter can oxidize another vanadium +III or +IV site after either migration over the surface [40] or desorption/readsorption of oxygen.

These results are supported by a joint experimental–computational study [25] that reported formation of peroxovanadate on exposure of a (reduced) V_2O_3 (0001) surface to molecular oxygen at low temperature (90 K) under UHV conditions. Under these conditions, the surface exhibited V^{III} sites. The peroxo groups decomposed into vanadyl groups between 170 K and room temperature.

It is important to stress that peroxovanadate is active for both propane and propene oxidation, and at the temperatures considered here (600–800 K), the oxidation rate is one to two orders of magnitude larger for propene than for propane at the same concentrations. Under these conditions, propene oxidation is 4–8 times slower than propane oxidation on vanadyl sites. The finding that the catalyst's capability for consecutive C_3H_6 oxidation to CO_x is significantly reduced when N_2O instead of O_2 is used as the oxidizing agent can be understood by keeping in mind that N_2O cannot form peroxovanadate. As shown in Fig. 9, the route of CO_x formation via propene reaction with peroxovanadates disappeares in the presence of N_2O.

Our theoretical results agree well with experimental observations. CO_x formed in the ODP reaction over VO (2.7 wt%)/MCM-41 stems mainly from consecutive propene oxidation [6,38]. Experimentally, direct propane oxidation to CO_x plays a minor role, and the catalyst's capability for consecutive C_3H_6 oxidation to CO_x is strongly reduced on replacement of O_2 with N_2O.

5. Conclusion

According to our calculations, different oxidants in the ODP reaction on supported vanadium oxide catalysts not only influence the degree of reduction of the VO_x species, but also may generate different concentrations of selective vanadyl and nonselective peroxo species, as illustrated in Fig. 9 for O_2 and N_2O. Propene is formed primarily from propane via oxidative dehydrogenation by lattice (vanadyl) oxygen of VO_x species. Vanadyl oxygen also is active for consecutive propene oxidation. Vanadyl groups can be restored via reoxidation by O_2 and N_2O. N_2O is less active and can oxidize V^{III} sites only, whereas O_2 can oxidize both V^{III} and V^{IV}. Only in the case of reoxidation by O_2 is the vanadyl oxygen species reached via a peroxovanadate precursor. The latter is more reactive for propene oxidation (leading to CO_x) compared with vanadyl species.

Acknowledgments

This work was supported by the Deutsche Forschungsgemeinschaft (DFG) within the Collaborative Research Center 546, "Structure, Dynamics and Reactivity of Transition Metal Oxide Aggregates." X.R. was supported through an Alexander von Humboldt fellowship. The authors thank Dr. Rémy Fortrie for fruitful discussions.

References

[1] E.A. Mamedov, V.C. Corberan, Appl. Catal. A 127 (1995) 1.

[2] O.V. Buyevskaya, M. Baerns, Catalysis 16 (2002) 155.
[3] M. Baerns, G. Grubert, E.V. Kondratenko, D. Linke, U. Rodemerk, Oil Gas-Eur. Mag. 1 (2003) 36.
[4] R.B. Watson, U.S. Ozkan, J. Catal. 191 (1999) 12.
[5] E.V. Kondratenko, M. Baerns, Appl. Catal. A 222 (2001) 133.
[6] E.V. Kondratenko, M. Cherian, M. Baerns, X. Su, R. Schlögl, X. Wang, I.E. Wachs, J. Catal. 234 (2005) 131.
[7] H.Y. Yamamoto, H.Y. Chu, M. Xu, C. Xu, C. Shi, J. Lunford, J. Catal. 142 (1993) 325.
[8] A.G. Anshits, V.G. Roguleva, E.V. Kondratenko, Stud. Surf. Sci. Catal. 82 (1994) 337.
[9] A.G. Anshits, E.V. Kondratenko, E.V. Voskresenskaya, L.I. Kurteeva, N.I. Pavlenko, Catal. Today 46 (1998) 211.
[10] G.I. Panov, A.K. Uriarte, M.K. Rokin, V.I. Sobolev, Catal. Today 41 (1998) 365.
[11] D. Hoenicke, V. Duma, W. Krysmann, DE 98-19854615, 1998, to CREAVIS GmbH.
[12] E.V. Kondratenko, M. Cherian, M. Baerns, Catal. Today 99 (2005) 59.
[13] A.D. Becke, J. Chem. Phys. 98 (1993) 5648.
[14] C. Lee, W. Yang, R.G. Parr, Phys. Rev. B 37 (1988) 785.
[15] A. Schäfer, C. Huber, R. Ahlrichs, J. Chem. Phys. 100 (1994) 5829.
[16] R. Ahlrichs, M. Bär, M. Häser, H. Horn, C. Kölmel, Chem. Phys. Lett. 162 (1989) 165.
[17] O. Treutler, R. Ahlrichs, J. Phys. Chem. 102 (1995) 346.
[18] K. Eichkorn, F. Weigend, O. Treutler, R. Ahlrichs, Theor. Chem. Acc. 97 (1997) 119.
[19] M. von Arnim, R. Ahlrichs, J. Chem. Phys. 111 (1999) 9183.
[20] R. Caballol, O. Castell, F. Illas, I.d.P.R. Moreira, J.P. Malrieu, J. Phys. Chem. A 101 (1997) 7860.
[21] X. Rozanska, R. Fortrie, J. Sauer, J. Phys. Chem. C 111 (2007) 6041.
[22] J. Döbler, M. Pritzsche, J. Sauer, J. Am. Chem. Soc. 127 (2005) 10861.
[23] D. Schröder, S. Shaik, H. Schwarz, Acc. Chem. Res. 33 (2000) 139.
[24] J.-L. Carreón-Macedo, J.N. Harvey, J. Am. Chem. Soc. 126 (2004) 5789.
[25] M. Abu Haija, S. Guimond, Y. Romanyshyn, A. Uhl, H. Kuhlenbeck, T.K. Todorova, M.V. Ganduglia-Pirovano, J. Döbler, J. Sauer, H.-J. Freund, Surf. Sci. 600 (2006) 1497.
[26] J.M. Wittbrodt, H.B. Schlegel, J. Chem. Phys. 105 (1996) 6574.
[27] J. Gräfenstein, A.M. Hjerpe, E. Kraka, D. Cremer, J. Phys. Chem. A 104 (2000) 1748.
[28] T. Hirao, Chem. Rev. 97 (1997) 2707.
[29] N. Magg, B. Immaraporn, J.B. Giorgi, T. Schroeder, M. Bäumer, J. Döbler, Z. Wu, E. Kondratenko, M. Cherian, M. Baerns, P.C. Stair, J. Sauer, H.-J. Freund, J. Catal. 226 (2004) 88–100.
[30] X. Rozanska, R. Fortrie, J. Sauer (2008) in preparation.
[31] S.L.T. Andersen, Appl. Catal. A 112 (1994) 209.
[32] A. Khodakov, B. Olthof, A.T. Bell, E. Iglesia, J. Catal. 181 (1999) 205.
[33] K. Chen, A. Khodakov, J. Yang, A.T. Bell, E. Iglesia, J. Catal. 186 (1999) 325.
[34] K. Chen, E. Iglesia, A.T. Bell, J. Catal. 192 (2000) 197.
[35] K. Chen, A.T. Bell, E. Iglesia, J. Phys. Chem. B 104 (2000) 1292.
[36] R. Grabowski, J. Sloczyñski, N.M. Grzesik, Appl. Catal. A 232 (2002) 277.
[37] E.V. Kondratenko, N. Steinfeldt, M. Baerns, Phys. Chem. Chem. Phys. 8 (2006) 1624.
[38] O. Ovsitser, M. Cherian, E.V. Kondratenko, J. Phys. Chem. C 111 (2007) 8594.
[39] J. Sauer, J.-R. Hill, Chem. Phys. Lett. 218 (1994) 333.
[40] A. Goodrow, A.T. Bell, J. Phys. Chem. C 111 (2007) 14753.